Published in final edited form as:

Neuron. 2016 September 21; 91(6): 1316–1329. doi:10.1016/j.neuron.2016.08.014.

Structural basis for negative allosteric modulation of GluN2A-containing NMDA receptors

Feng Yi[1,2], **Tung-Chung Mou**[1,3,4], **Katherine N. Dorsett**[2], **Robert A. Volkmann**[5], **Frank S. Menniti**[6], **Stephen R. Sprang**[3,4], and **Kasper B. Hansen**[2,3]

[2]Department of Biomedical and Pharmaceutical Sciences, University of Montana, Missoula, MT 59812, USA.

[3]Center for Biomolecular Structure and Dynamics, University of Montana, Missoula, MT 59812, USA.

[4]Division of Biological Sciences, University of Montana, Missoula, MT 59812, USA.

[5]BioPharmaWorks, LLC, Groton, CT 06340, USA.

[6]MindImmune Therapeutics, Inc., and George & Anne Ryan Institute for Neuroscience, Kingston, RI 02881, USA.

Summary

NMDA receptors mediate excitatory synaptic transmission and regulate synaptic plasticity in the central nervous system, but their dysregulation is also implicated in numerous brain disorders. Here, we describe GluN2A-selective negative allosteric modulators (NAMs) that inhibit NMDA receptors by stabilizing the *apo*-state of the GluN1 ligand binding domain (LBD), which is incapable of triggering channel gating. We describe structural determinants of NAM binding in crystal structures of the GluN1/2A LBD heterodimer, and analyses of NAM-bound LBD structures corresponding to active and inhibited receptor states reveal a molecular switch in the modulatory binding site that mediate the allosteric inhibition. NAM binding causes displacement of a valine in GluN2A and the resulting steric effects can be mitigated by the transition from glycine-bound to *apo*-state of the GluN1 LBD. This work provides mechanistic insight to allosteric NMDA receptor

Correspondence: Kasper B. Hansen (kasper.hansen@mso.umt.edu).

[1]Co-first author.

Accession numbers

Coordinates and structure factors for the glycine/glutamate-bound GluN1/2A LBD structure (5I57) and the complexes with TCN-201 (5I56), MPX-004 (5I58), and MPX-007 (5I59), as well as the DCKA/glutamate-bound GluN1/2A LBD structure in complex with MPX-007 (5JTY) have been deposited in the Protein Data Bank.

Supplemental Information

Supplemental Information includes eight figures, three tables, and Supplemental Experimental Procedures.

Author Contributions

F.Y., K.N.D., and K.B.H. designed and performed electrophysiology experiments and analyzed the data. T.-C.M. designed and performed crystallographic experiments and analyzed the data. R.A.V. and F.S.M. designed experiments and provided MPX-004/MPX-007 for the study. S.R.S. designed crystallographic experiments and analyzed the data. All authors contributed to interpreting the data and writing the paper.

inhibition, thereby facilitating the development of novel classes NMDA receptor modulators as therapeutic agents.

Introduction

NMDA receptors are ligand-gated ion channels that mediate a component of the synaptic response to glutamate, and are principal regulators of synapse formation and synaptic plasticity in the central nervous system (CNS) (Traynelis et al., 2010). Given these essential roles, dysfunction of NMDA receptors is implicated in multiple CNS disorders and the receptors have been intensively studied as targets in the development of new therapeutic agents (Paoletti et al., 2013; Traynelis et al., 2010).

The majority of NMDA receptors in the CNS contains two glycine-binding GluN1 subunits and two glutamate-binding GluN2 subunits (Karakas and Furukawa, 2014; Lee et al., 2014), and requires simultaneous binding of glycine (or D-serine) and glutamate for activation (Benveniste and Mayer, 1991). NMDA receptor gating is triggered by synaptic release of glutamate, which occurs on a millisecond timescale, whereas extracellular glycine (or D-serine) is constitutively present at saturating or sub-saturating concentrations. The GluN1 subunit is encoded by a single gene processed to yield eight splice variants, while there are four GluN2 subunits (GluN2A-D) encoded by separate genes (Traynelis et al., 2010). The GluN2 subunits endow NMDA receptors with distinct functional and pharmacological properties (Gielen et al., 2009; Monyer et al., 1994; Vicini et al., 1998; Yuan et al., 2009) and are differentially expressed in circuits, neurons, and subcellular compartments during CNS development and in the mature brain (Akazawa et al., 1994; Ishii et al., 1993; Monyer et al., 1994). Thus, the physiological roles of NMDA receptors are finely tuned by the two GluN2 subunits included in the tetrameric receptor complex. Ligands with selectivity towards different GluN2 subunits are useful tools to probe the function of different NMDA receptor subtypes in the CNS and can have unique therapeutic potentials. In this regard, recent genetic analyses have implicated variation in the gene encoding GluN2A (*GRIN2A*) in childhood epilepsy/aphasia syndromes (reviewed in Yuan et al., 2015). A large subset of these *GRIN2A* mutations is gain-of-function (i.e. they increase the activity of GluN2A-containing NMDA receptors) that cause severe neurologic complications, including early-onset epileptic encephalopathy and refractory seizures (e.g. see Pierson et al., 2014; Yuan et al., 2014).

Bettini et al. (2010) described the first class of GluN2A-selective non-competitive NMDA receptor antagonists. TCN-201, the prototypical member of this class, is a negative allosteric modulator (NAM) of glycine binding to the GluN1 subunit (Hansen et al., 2012). Glycine also negatively modulates TCN-201 binding and elevated glycine concentrations surmounts non-competitive TCN-201 inhibition, which may limit the usefulness of TCN-201 in studies of neuronal GluN2A-containing NMDA receptors (Bettini et al., 2010; Edman et al., 2012; Hansen et al., 2012). Recently, the binding site for an analog of TCN-201 was identified at the interface between GluN1 and GluN2A subunits in crystal structures of the GluN1/2A ligand binding domain (LBD) heterodimer (Hackos et al., 2016). Crystal structures also revealed that GluN2A-selective positive allosteric modulators can target the GluN1-GluN2A

dimer interface with a binding site that overlaps with the NAM binding site (Hackos et al., 2016; Volgraf et al., 2016). Thus, this recent crystallographic data establish the GluN1/GluN2 LBD interface as a locus for both negative and positive allosteric modulation of NMDA receptors by small-molecule ligands. However, the molecular mechanisms by which ligand binding to this new modulatory site cause inhibition or potentiation are still unresolved.

Here, we take advantage of structural and pharmacological differences between TCN-201 and two recently described analogs, MPX-004 and MPX-007 (Volkmann et al., 2016), to investigate the molecular mechanism for GluN2A-selective allosteric inhibition of glycine binding. Using an engineered disulfide bond, we show that NAM binding stabilizes the glycine-lacking, *apo*-state of the GluN1 LBD, and that allosteric inhibition requires a transition from the glycine-bound to the *apo*-state of the GluN1 LBD. Furthermore, we report crystal structures of NAMs bound to the glycine/glutamate-bound GluN1/2A LBD heterodimer as well as the DCKA/glutamate-bound GluN1/2A LBD heterodimer, which correspond to the active and inhibited states of the NMDA receptor, respectively. Comparison of these structures reveals the molecular switch in the NAM binding site that mediates allosteric inhibition and provides broader insight into bidirectional modulation of NMDA receptors by NAMs and PAMs binding at this modulatory site.

Results

Glycine-sensitivity is different among GluN2A-selective NAMs

Recently, the chemical scaffold of TCN-201 was modified to yield MPX-004 and MPX-007 (Volkmann et al., 2016) (Figure 1A). We evaluated GluN2A-selectivity and potency of TCN-201, MPX-004, and MPX-007 at recombinant NMDA receptors containing GluN1 and either GluN2A, GluN2B, GluN2C or GluN2D (i.e. diheteromeric GluN1/2A-D receptors). The three NAMs are equally potent (IC_{50} values of approx. 200 nM) and produce nearly complete inhibition of GluN1/2A receptors activated by 100 μM glutamate plus 3 μM glycine (Figure 1 and Table S1). TCN-201 and MPX-004 exhibit strict selectivity for GluN1/2A over GluN1/2B-D receptor subtypes, whereas MPX-007 inhibits GluN1/2B-D receptors at higher concentrations (10-30 μM) (Figure S1). Notably, 30 μM MPX-007 inhibits GluN1/2B receptors by 48% ± 3% (n = 6) in the presence of 3 μM glycine.

TCN-201 negatively modulates glycine binding to the GluN1 subunit and inhibition by TCN-201 is sensitive to the concentration of extracellular glycine (Hansen et al., 2012). The selectivity and structural similarity of TCN-201, MPX-004, and MPX-007 suggest they share this mechanism of action (Volkmann et al., 2016). To compare the glycine-sensitivity of the NAMs, we determined potency and efficacy for inhibition of GluN1/2A in the presence of 1-300 μM glycine (Figure 1C). The inhibitory potency of TCN-201 decreases with increasing extracellular glycine concentrations, and TCN-201 inhibition is markedly diminished in 300 μM glycine (Table S1). MPX-004 inhibition is less sensitive to glycine compared to TCN-201, and the IC_{50} increases only by 3.8-fold in 30 μM glycine compared to in 3 μM glycine. However, maximal inhibition by MPX-004 is incomplete in 300 μM glycine (71% ± 4%; n = 6; Table S1). Inhibition by MPX-007 has the lowest sensitivity to glycine, and the IC_{50} increases by 3.2-fold in 30 μM compared to in 3 μM glycine (Table

S1). Furthermore, maximal inhibition by MPX-007 of responses in 300 μM glycine is nearly complete (95% ± 1%; n = 5; Table S1). These results demonstrate a structure-activity relationship for this class of NAMs with respect to their allosteric interaction with glycine binding.

Increased GluN2A expression during CNS development is accompanied by the appearance of triheteromeric GluN1/2A/2B receptors, which contain two GluN1, one GluN2A, and one GluN2B subunit (Rauner and Kohr, 2011; Sheng et al., 1994) and have distinct functional and pharmacological properties compared to diheteromeric GluN1/2A and GluN1/2B receptors (Cheriyan et al., 2016; Hansen et al., 2014; Hatton and Paoletti, 2005; Stroebel et al., 2014; Tovar et al., 2013). We determined NAM potency and efficacy at recombinant triheteromeric GluN1/2A/2B in the presence of 1-300 μM glycine (Figure 1D and Table S1). The triheteromeric GluN1/2A/2B receptors were expressed as previously described (Hansen et al., 2014) (Figure S2). At low glycine (1-3 μM), all three NAMs produce strong inhibition of GluN1/2A/2B. Furthermore, NAM inhibition of GluN1/2A/2B exhibits the same rank order of sensitivity to glycine as observed for GluN1/2A, with TCN-201 being most sensitive and MPX-007 being least sensitive (Figure 1D and Table S1). Complete inhibition of GluN1/2A/2B by the NAMs is consistent with a requirement for both GluN1 glycine binding sites to be occupied for channel gating (Benveniste and Mayer, 1991). We also note that at each glycine concentration, the potency for inhibition of GluN1/2A/2B is reduced relative to that for GluN1/2A. This may simply reflect the requirement to inhibit only one of the two GluN1/2A dimers in diheteromeric GluN1/2A receptors. However, the potency shift may also be indicative of a change in NAM affinity caused by one GluN1/2B dimer affecting the conformation of the GluN1/2A dimer in triheteromeric GluN1/2A/2B receptors.

Crystal structures of the binding site for negative allosteric modulation

Site-directed mutagenesis has identified residues in the subunit interface between GluN1 and GluN2A LBDs that influence TCN-201 inhibition and in particular, Val783 in GluN2A was identified as critical for TCN-201 binding (Hansen et al., 2012). Recently, the interaction between an analog of TCN-201 (“compound 6”; Bettini et al., 2010) and GluN2A V783 was shown in a crystal structure of the isolated GluN1/2A LBD heterodimer (Hackos et al., 2016). Here, we show that TCN-201, MPX-004, and MPX-007 bind this same modulatory binding site.

We determined the glycine/glutamate-bound GluN1/GluN2A LBD heterodimer structure at 1.70 Å resolution, and three structures of the glycine/glutamate-bound GluN1/GluN2A LBD heterodimer in complex with TCN-201 (2.28 Å), MPX-004 (2.52 Å), or MPX-007 (2.11 Å) (Figure 2 and Table S2). The agonist-bound GluN1/GluN2A LBD structure at 1.70 Å is virtually identical to the previously published structure at 1.86 Å (root-mean-square deviation of 0.151 Å over 501 Cα atoms; PDB ID 4NF8) (Jespersen et al., 2014). The NAMs occupy a binding site located in the subunit interface between GluN1 and GluN2A LBDs. Notably, binding of the agonists, glutamate and glycine, was seemingly unaffected by NAM occupancy and remained bound to their respective agonist binding sites in the NAM-bound structures (Figure 2B). Thus, these crystal structures confirm that TCN-201 and the

related NAMs can bind to the GluN1/GluN2A LBDs in which glutamate and glycine are also bound, consistent with previous functional analyses (Hansen et al., 2012). The NAMs adopt a remarkable hairpin-like conformation in the binding site with the distal halogenated aromatic ring (ring A) forming a stacking, parallel-displaced, sandwich with the middle aromatic ring (ring B), which is a phenyl ring in TCN-201 and a pyrazine ring in MPX-004 and MPX-007 (Figures 2D and 2E). The same conformation was observed for compound 6 in Hackos et al. (2016).

The NAM binding site is lined by residues from β-sheet 10 and α-helices J and K in GluN2A on one side of the dimer interface and β-sheets 10 and 14 in GluN1 on the other side (Figure 2F). In both GluN1 and GluN2A, β-sheets 10 and 14 connect the two lobes in the kidney-shaped LBDs and serve as a hinge for the transition from the open to closed LBD conformation in response to agonist binding, which is the initial conformational change that triggers ion channel gating (Furukawa et al., 2005; Jespersen et al., 2014). The NAMs are pinned between the hinge region of GluN1 and the apex of GluN2A helix J (i.e. C-terminus of helix J), which interacts with helix F in the lower lobe of the GluN1 LBD. Helix F undergoes large movements during transitions between open and closed LBD conformations (Jespersen et al., 2014). The NAM binding site is therefore positioned to influence the dynamic behavior of agonist-induced conformational changes in the GluN1 LBD.

NAM binding contacts in the modulatory binding site

The crystal structures reveal contacts between the side chain of GluN2A V783 at the apex of helix J and the middle ring B in the NAM ligands (Figures 2F-H). GluN2A-selectivity is, to a large extent, explained by steric occlusion of NAM binding to GluN2B and GluN2C/D, since these subunits have larger phenylalanine and leucine, respectively, at the position of GluN2A V783 (Hackos et al., 2016; Hansen et al., 2012) (Figure S3). At the other side of the sandwich formed by NAM rings A and B, is the aromatic ring of GluN1 Y535, which forms an edge-to-face interaction with NAM ring A. GluN1 Y535 is located in β-sheet 10 of the hinge region, and the shape and properties of this residue influence receptor deactivation time course of both glutamate and glycine binding sites (Borschel et al., 2015; Furukawa et al., 2005). Interestingly, the sulfonyl groups in the NAM ligands do not form polar interactions, but are located within van der Waals contact distance to aliphatic carbons from GluN1 I519, P532, and G757 and GluN2A P527 (Figures 2F-H). Similar nonpolar interactions between protein and ligand sulfonyl groups are commonly found in crystal structures (Bissantz et al., 2010). The three NAMs display relatively subtle variation in binding contacts, and such differences are mainly mediated by the structural differences in NAM rings B and C (Figure 2 and Figure S4).

NAM-mediated structural changes in the agonist-bound GluN1/GluN2A LBD heterodimer

Structural superposition of the NAM-bound structures with the NAM-lacking structure show they are nearly identical with root-mean-square deviation of 0.233 Å (509 Cα atoms), 0.266 Å (463 Cα atoms), and 0.263 Å (451 Cα atoms) for TCN-201, MPX-004, and MPX-007, respectively. Close inspection of residues surrounding the NAM binding site reveals that the side chain of GluN2A E530 adopts a different conformation to accommodate NAM binding (Figure S4). However, the most striking difference is a shift in the position of V783 at the

apex of helix J in GluN2A (Figure 3A). GluN2A V783 is in close contact with ring B of the NAM ligands and there is an incremental displacement of the GluN2A V783 side chain among the three NAM-bound structures ranging from 0.5 Å to 1.0 Å, which parallels the potency and efficacy of the NAMs (i.e. TCN-201 < MPX-004 < MPX-007). The largest displacement of GluN2A V783 occurs in the complex with MPX-007, of which the methyl substituent on the pyrazine ring B is in Van der Waals contact with the backbone carbonyl of GluN2A P527 (Figure 3A). The side chain of GluN2A V783 prevents rotation of the pyrazine ring B in MPX-007, which could mitigate the repulsive contact between the non-polar methyl group of MPX-007 and the polar backbone carbonyl of GluN2A P527. Furthermore, the side chain of GluN2A V783 is in contact with GluN1 F754, and the NAM-mediated displacement of GluN2A V783 is accompanied by a ~20-30° rotation of the aromatic ring of GluN1 F754 (Figure 3A). We suggest that the more extensive displacement of GluN2A V783 and accompanying steric effect on GluN1 F754 may account for the increased efficacy of MPX-007 compared to TCN-201 and MPX-004 at higher glycine concentrations. Analysis of the human glycine/glutamate-bound GluN1/2A LBD heterodimer structures described by Hackos et al. (2016) reveals that “compound 6” displaces GluN2 V783 by 0.7 Å, similar to TCN-201, MPX-004, and MPX-007 in the rat structures reported here.

Since the displacements of GluN2A V783 identified using structural superposition are relatively small (0.5-1.0 Å) compared to the crystallographic resolution (1.70-2.52 Å), we used difference distance map analysis to gain further insight into GluN2A V783 movement and to identify additional distributed structural changes in the GluN1 LBD. For NAM-lacking and NAM-bound structures, we measured distances between Cα atoms (D_{ij}) in helices J and K of GluN2A (residues 766-796) and the lower lobe of the GluN1 LBD as well as helix D and β-sheets 10 and 14 (residues 510-544 and 665-770) (Figure S5). Pairs of Cα atoms with distances less than 15 Å were identified in each structure, as this distance corresponds to that between GluN2A V783 and glycine bound in the GluN1 LBD. For these pairs of Cα atoms, the distance measured in the NAM-lacking structure was subtracted from the distance measured in each of the NAM-bound structures. Absolute distance differences $|\Delta D_{ij}|$ of more than 0.5 Å were then mapped to reveal relative movements of residues in response to NAM binding (Figure 3B).

The difference distance maps yielded three main observations. First, NAM binding produces a movement at the apex of helix J in GluN2A, including V783, away from β-sheets 10 and 14 in the GluN1 hinge region (e.g. Y535 and R755) (Figure 3A). The relative positioning of GluN2A helix J and GluN1 helix F also change in response to NAM binding. Second, TCN-201 binding produces a distinct difference distance map compared to MPX-004 and MPX-007 binding (Figure 3B). TCN-201 mainly induces a separation between GluN2A V783 and the hinge region in GluN1 (β-sheets 10 and 14), whereas binding of MPX-004 or MPX-007 results in additional separation of GluN2A helix J and GluN1 helix F (Figure 3B). Third, the magnitude of the displacements revealed by the difference distance maps increases with TCN-201 displaying the smallest movements and MPX-007 the largest (Figure 3B). This trend mirrors the rank-order of NAM potency and efficacy (i.e. TCN-201 < MPX-004 < MPX-007).

In summary, the structural analyses show that NAM binding produces a “push” on GluN2A V783 that leads to a small separation between the apex of GluN2A helix J and the GluN1 hinge region and helix F. We hypothesize that these structural changes can destabilize the glycine/glutamate-bound GluN1/GluN2A LBD heterodimer structure.

GluN2A-selective NAMs stabilize the *apo*-state of the GluN1 LBD

We have previously reported that high concentrations of glycine can activate responses from TCN-201-bound GluN1/2A receptors with a strikingly accelerated deactivation time course (Hansen et al., 2012). These results support a mechanism where NAMs inhibit receptor activation by interfering with glycine binding. However, this does not preclude additional NAM interference with downstream conformational changes that trigger ion channel gating following agonist-induced closure of the GluN1 LBD. To investigate this possibility, we designed experiments using an engineered disulfide bond that locks the GluN1 LBD in the closed conformation, mimicking the effect of glycine binding (Kussius and Popescu, 2010) (Figure S6). If NAM binding directly disrupts gating, then the inhibitory activity should be preserved, at least to some extent, in disulfide-crosslinked receptors.

Co-expression of the crosslinked GluN1 mutant (GluN1-N499C+Q686C; hereafter GluN1-CC) with GluN2A produces receptors that are activated by glutamate alone and are not potentiated by addition of glycine (see also (Kussius and Popescu, 2010) (Figures 4A-C). The glutamate-activated responses also are not sensitive to the competitive glycine site antagonist 7CKA (Figure 4C), which stabilizes the open GluN1 LBD conformation (Furukawa and Gouaux, 2003; Jespersen et al., 2014). Significantly, glutamate-activated responses from crosslinked GluN1-CC/2A are not inhibited by NAMs (Figures 4B and 4C), indicating that NAM inhibition requires opening of the GluN1 LBD. Addition of DTT to the extracellular recording solution to reduce disulfide bonds in GluN1-CC/2A had no effect on the amplitude of glutamate-activated responses, but restored the ability of 7CKA to inhibit such responses (Figures 4D-F). This suggests that the engineered disulfide bond is reversibly, but transiently, reduced by DTT, thereby retaining activation by glutamate in the nominal absence of glycine. However, transient reduction by DTT allows access of 7CKA to bind and stabilize the open GluN1 LBD, which inhibits the glutamate response. Importantly, similar co-application of DTT and NAM also restores inhibition, further demonstrating that NAMs require opening of the GluN1 LBD for inhibition (Figures 4E and 4F). The possibility that the NAMs are incapable of binding to crosslinked GluN1-CC/2A receptors due to limited access to the binding pocket is unlikely, since we observed that MPX-004 produces a significant potentiation of glutamate-activated responses in crosslinked receptors (Figure 4C).

The experiments using the engineered disulfide bond demonstrate that the NAMs stabilize an open state of the GluN1 LBD, which is incapable of triggering ion channel gating. This also implies that the NAM-bound GluN1/2A LBD structures shown in Figure 2, with glycine bound to the closed state of the GluN1 LBD, correspond to the low-affinity NAM binding site.

Mechanism of allosteric inhibition by GluN2A-selective NAMs

To identify interactions in the NAM binding site that change during transitions between closed and open states of the GluN1 LBD (i.e. low- and high-affinity NAM binding), we determined the structure of the DCKA/glutamate-bound GluN1/2A LBD heterodimer in complex with MPX-007 at 2.70 Å (Figure 5 and Table S2). In this structure, the competitive glycine site antagonist DCKA stabilizes the open state of the GluN1 LBD, which is similar to the conformation of the *apo*-form (Furukawa and Gouaux, 2003; Jespersen et al., 2014; Yao et al., 2013) (Figure 5B). Thus, this structure with MPX-007 bound to the glycine-lacking GluN1/2A LBD heterodimer corresponds to an inactive state of the NMDA receptor with high-affinity NAM binding (Figure 5A). The structure of the DCKA/glutamate-bound GluN1/2A LBD heterodimer (in the absence of a NAM) has been previously published (PDB ID 4NF4; Jespersen et al., 2014). Thus, there is crystallographic data for all states in the NAM allosteric inhibition cycle (Figure 5). From these structural data, we deduce a mechanism for allosteric inhibition by the NAMs that accounts for the transition from low to high NAM affinity upon glycine unbinding.

As described above, binding of NAM (i.e. MPX-007) displaces GluN2A V783, which results in steric push on the side chain of GluN1 F754 (Figure 6A) and a separation between the apex of GluN2A helix J and the GluN1 hinge region (Figure 3B). We hypothesize that these structural changes destabilize the glycine/glutamate-bound GluN1/GluN2A LBD heterodimer structure, and support this hypothesis by demonstrating that NAMs stabilize the *apo*-state of the GluN1 LBD (Figure 4). In the open state of the GluN1 LBD (stabilized by DCKA), the side chain of GluN1 F754 swings ~90 degrees way from GluN2A V783, and is therefore not in position to sterically hinder the NAM-mediated “push” on GluN2A V783 (Figure 6B). We hypothesize that this state accounts for high affinity NAM binding. When NAM is bound, the loss of contact between GluN2A V783 and GluN1 F754 is virtually the only change that occurs in the vicinity of the NAM ligand during opening of the GluN1 LBD and glycine unbinding. Thus, the contact between GluN2A V783 and GluN1 F754 forms a molecular switch in the modulator binding site, which mediates the transition from low- to high affinity NAM binding, and thereby allosteric inhibition. Specifically, glycine binding stabilizes the closed GluN1 LBD conformation and thereby forces contact between GluN2A V783 and GluN1 F754, resulting in low-affinity NAM binding (Figure 6A). By contrast, the open GluN1 LBD and glycine unbinding enables a loss of contact between GluN2A V783 and GluN1 F754, resulting in high-affinity NAM binding (Figure 6B). Electron density maps for ligands and residues implicated in the allosteric mechanism are shown in Figure S7.

The allosteric nature of NAM inhibition is further revealed by comparison of structures of the DCKA-stabilized GluN1 LBD with or without NAM binding. Unbinding of NAM from the glycine-lacking GluN1/GluN2A LBD heterodimer (stabilized by DCKA) is not accompanied by movement of GluN2A V783, but rather GluN1 Y535, S756, and Q536 in the hinge region relax to markedly different conformations (Figure 6C). Interestingly, the conformations of GluN1 Y535, S756, and Q536 that are stabilized by NAM binding are similar to those observed when glycine is bound in the absence of NAM (Figure 6D). Thus, NAM binding stabilizes a conformation of the GluN1 hinge region that is similar to the

conformation in the glycine-bound state (Figures 6B-D). In fact, relaxation of GluN1 S756 upon glycine unbinding is sterically occluded by NAM binding (Figure 6C). This observation suggests that NAM binding requires a conformation of the GluN1 hinge region that is similar to the glycine-bound, closed state of the GluN1 LBD, thereby enabling NAM binding to glycine-bound NMDA receptors and preventing the mechanism of inhibition from being strictly competitive.

GluN2A V783 and GluN1 F754 influence glycine potency in GluN1/2A receptors

In the absence of NAM, the contact between GluN2A V783 and GluN1 F754 is reformed when glycine binds, resulting in a movement of GluN2A V783 in the opposite direction compared to the NAM-mediated “push” (Figure 6D). Since GluN2A V783 and GluN1 F754 are implicated in allosteric inhibition of glycine binding, we hypothesize that the contact between these residues can influence glycine potency in GluN1/2A receptors. We therefore mutated these residues in GluN1/2A receptors and determined glycine potency (Figure 7). We found an inverse correlation between glycine EC_{50} and the size of the side chain at the position of GluN2A V783; glycine EC_{50} values are 2.26 μM, 0.52 μM, and 0.38 μM for V783A, V783L, and V783F, respectively, compared to 1.1 μM for wild type GluN1/2A (Table S3). In the absence of NAM, the influence of GluN2A V783 on glycine potency should be mediated through van der Waals contact with GluN1 F754 (Figures 6D and 7A). Consistent with this, substitution of GluN1 F754 with leucine or valine, which have progressively smaller side chains, increased glycine EC_{50} (i.e. reduced glycine potency) to 16.5 μM and 21.5 μM, respectively (Figure 7B and Table S3).

In summary, mutational analyses of GluN2A V783 and GluN1 F754 demonstrate that these residues influence glycine potency in GluN1/2A receptors, despite their location 16 Å and 13 Å, respectively, away from the glycine agonist (Cα-Cα distance). This result supports the interpretation that the contact between GluN2A V783 and GluN1 F754 mediate allosteric interaction between glycine and NAM binding sites (i.e. they form the molecular switch).

Functional evidence for the GluN2A V783/GluN1 F754 molecular switch

In order to provide functional evidence to support our interpretation of the crystallographic data, we used Schild analysis in combination with a previously described operational model for allosteric modulation of glycine binding (Hansen et al., 2012). In this model, the glycine binding affinity (K_A) is reduced by an allosteric constant α upon NAM binding, and NAM binding affinity (K_B) is reciprocally reduced by α upon glycine binding (Figure 8A). Analysis of glycine concentration-response relationships for wild type GluN1/2A receptors in the absence or presence of TCN-201 yields the glycine potency in the absence of modulator (EC_{50} = 1.1 μM), TCN-201 binding affinity in the absence of glycine (K_B = 27 nM), and the allosteric constant (α = 0.007) (Figures 8A-C and Table S3). Thus, TCN-201 binds with high affinity (K_B = 27 nM) in the absence of glycine and with low affinity (K_B/α = 3.7 μM) when glycine is bound.

The aromatic ring of GluN1 Y535 forms an edge-to-face interaction with ring A of the NAM ligands and this interaction is not changing during the transition between open and closed LBD conformational states. Compared to wild type GluN1/2A, the binding affinity K_B and

the allosteric constant are virtually unchanged for the GluN1-Y535F substitution, which preserves the aromatic ring (Figure 8D and Table S3). By contrast, removal of the edge-to-face interaction by the GluN1-Y535L substitution increases K_B to 76 nM and modestly increases the allosteric constant to 0.016 (Figure 8E and Table S3). Thus, the GluN1-Y535L mutation reduces TCN-201 binding affinity without a strong effect on the allosteric constant. This is consistent with observations from crystallographic data, which show that the edge-to-face interaction is conserved in both open (DCKA-bound) and closed (glycine-bound) GluN1 LBD conformations. Thus, the functional data support that NAM inhibition is not mediated by a conformational change of the GluN1 Y535 side chain.

Schild analysis showed that the GluN1-F754L substitution produces little to no change in TCN-201 binding affinity K_B, but increases the allosteric constant to 0.018 (Figure 8F and Table S3). The GluN1-F754V substitution increased both K_B to 131 nM and the allosteric constant to 0.086 (Figure 8G and Table S3). Thus, substitutions of GluN1 F754 that are expected to diminish the contact with GluN2A V783 also reduce the difference between TCN-201 binding affinities in the open (DCKA-bound) and closed (glycine-bound) GluN1 LBD conformations (i.e. the allosteric constant increases). This is indicative of a diminished negative allosteric interaction between TCN-201 and glycine binding, suggesting that the GluN1-F754V substitution reduces the efficacy by which the NAM-mediated “push” on GluN2A V783 destabilizes the glycine-bound state of the GluN1 LBD. TCN-201 can maximally increase the glycine EC_{50} for wild type GluN1/2A by 143-fold (i.e. $1/\alpha$ = 1/0.007), but only by 12-fold (1/0.086) for receptors with the GluN1-F754V substitution. The functional data therefore further corroborate that GluN2A V783 and GluN1-F754 are key mediators of allosteric inhibition by forming the molecular switch that stabilizes the *apo*-state of the GluN1 LBD in the presence of NAM.

The side chain of GluN1 R755 forms extensive non-polar interactions with the NAM ligands and forms a salt bridge with GluN2A E792 across the dimer interface (Figure S4). It has previously been shown that mutations of GluN1 R755 affect the inhibitory potency of “compound 6” and TCN-201 (Hackos et al., 2016; Hansen et al., 2012), but effects on NAM binding affinity have not been evaluated. We mutated GluN1 R755 to lysine, which preserves the charge, and to alanine, which removes the side chain. The GluN1-R755K substitution increases TCN-201 binding affinity K_B to 1.9 μM compared to 27 nM at wild type GluN1/2A , and the GluN1-R755A substitution abolished TCN-201 inhibition (Figure S8 and Table S3). Thus, the side chain of GluN1 R755 is critical for TCN-201 binding.

Mutations of GluN2A V783 also clearly affect the inhibitory potency of “compound 6” and TCN-201 (Hackos et al., 2016; Hansen et al., 2012). We interrogated the effects of amino acid substitutions at GluN2A V783 on TCN-201 binding affinity (Figure S8 and Table S3). The GluN2A-V783A substitution modestly increases K_B to 79 nM, but also decreases the allosteric constant to almost 0 (α = 0.001; Figure S8 and Table S3). GluN2A-V783F and GluN2A-V783L substitutions produce stronger effects on TCN-201 binding affinity; K_B increased to 186 nM and 1.9 μM, respectively, but the allosteric constants could not be determined (Figure S8 and Table S3). The effects of amino acid substitutions at GluN2A-V783 on TCN-201 binding are important in considering subunit selectivity. The residue at the position of GluN2A V783 is phenylalanine in GluN2B and leucine in GluN2C/D (Figure

S3). The rank order of inhibitory efficacy for MPX-007 at NMDA receptor subtypes (GluN2A > GluN2B >> GluN2C/D) correlates with the effects on TCN-201 affinity for GluN2A V783 substitutions to analogous residues in GluN2B and GluN2C/D (V783 (2A) > V783F (2B) >> V783L (2C/D). This correlation further supports previous studies that implicate GluN2A V783 as a critical determinant of NAM subunit-selectivity (Hackos et al., 2016; Hansen et al., 2012). We found that MPX-007 inhibition of GluN1/2B receptors is also sensitive to the glycine concentration (Figure S1), suggesting that an analogous interaction between the phenylalanine residue in GluN2B and GluN1 F754 likely accounts for the mechanism of MPX-007 inhibition in this NMDA receptor subtype.

Discussion

Our studies reveal structural and mechanistic features of a modulatory site located at the subunit interface between GluN1 and GluN2 LBDs. We demonstrate that NAM binding to the modulatory site stabilizes the open conformation of the GluN1 LBD, thereby facilitating glycine unbinding and receptor inactivation. That is, NAM inhibition is primarily caused by disruption of glycine binding to the GluN1 subunit, which is conserved in all NMDA receptors. At the same time, residues that are non-conserved among GluN2 subunits enable NAM selectivity with respect to NMDA receptor subtypes. Analyses of NAM-bound and NAM-lacking GluN1/2A LBD heterodimer structures corresponding to active and inactive NMDA receptors reveal that GluN2A V783 and GluN1 F754 play principal roles in the allosteric mechanism and subunit-selectivity. The transition from low- to high-affinity NAM binding is enabled by glycine unbinding and opening of the GluN1 LBD and is mediated by the loss of contact between GluN2A V783 and GluN1 F754. By contrast, glycine binding stabilizes the closed GluN1 LBD and thereby forces contact between GluN2A V783 and GluN1 F754, resulting in low-affinity NAM binding. The contact between GluN2A V783 and GluN1 F754 is therefore the molecular switch that controls the difference between low- and high-affinity NAM binding, and this difference is the primary driving force for allosteric inhibition. The strong GluN2A-selectivity of TCN-201 and analogs is accounted for by steric occlusion of NAM binding to GluN2B-D subunits, where the amino acids that occupy the GluN2A V783 position are larger phenylalanine and leucine.

The NAM-bound GluN1/2A LBD structures, in which glycine remained bound and the GluN1 LBD adopted a closed conformation, correspond to active GluN1/2A receptors with NAM bound in a low affinity conformation. Interactions in the crystal lattice may favor a closed GluN1 LBD conformation over the glycine-free open conformation. Furthermore, the GluN1 LBD conformation (i.e. open and closed) is tightly coupled to opening and closing of the ion channel gate (Kazi et al., 2014; Kussius and Popescu, 2010), and removal of this interaction (i.e. in the isolated, soluble GluN1 LBD) could also favor the closed conformation of the GluN1 LBD in crystal structures. The GluN1 LBD also bound glycine and adopted the closed conformation in the previously described human GluN1/2A LBD heterodimer structure in complex with “compound 6” (Hackos et al., 2016).

Hackos et al. (2016) recently reported GluN1/2A LBD heterodimer structures in complex with GluN2A-selective positive allosteric modulators (PAMs) (see also (Volgraf et al., 2016). The NAM and PAM binding sites overlap and both classes of modulators interact

with GluN2A V783. However, PAM binding has no effect on the position of GluN2A V783 or on glycine potency for GluN1/2A, in stark contrast to the effects of the NAMs reported here. Rather, PAM binding increases NMDA receptor open probability and enhances glutamate potency, which results in slower receptor deactivation following removal of glutamate (Hackos et al., 2016; Volgraf et al., 2016). Close inspection of the GluN1/2A LBD heterodimer structures reported by Hackos et al. (2016) reveals that PAM binding results in a markedly different conformation of GluN1 Y535. This residue can interact with the GluN2A hinge region, and mutations of GluN1 Y535 produce strong effects on open probability and glutamate deactivation (Borschel et al., 2015; Furukawa et al., 2005). This suggests that the effects of PAM binding could be mediated through interactions with GluN1 Y535 and the GluN2A hinge region (Volgraf et al., 2016), and it is tempting to speculate that PAM binding stabilizes the fully closed GluN2A LBD, which is permissive for channel gating. By contrast, glutamate potency is not affected by the GluN2A-selective NAMs (Hansen et al., 2012), and we show here the conformation of GluN1 Y535 is not changed by NAM binding. Thus, the modulatory binding site at the GluN1/GluN2 LBD interface accommodates both PAMs and NAMs, and the valence of modulation depends on the displacement of specific residues within this site. We anticipate that future studies will reveal additional small molecule modulators and modes of modulation at this critical structural junction of the NMDA receptor.

The PAM/NAM binding site at the subunit interface in the GluN1/2A LBD heterodimer represents only the second binding site for small-molecule NMDA receptor modulators for which crystallographic data has been described. The other modulatory site binds GluN2B-selective antagonists, such as ifenprodil, and is located in the subunit interface between GluN1 and GluN2B amino-terminal domains (Karakas et al., 2011). The use of ifenprodil and its analogs as pharmacological tools has enabled precise localization of GluN2B-containing receptors in the CNS, and identified a wide range of normal processes and neurological diseases that involve GluN2B. In this regard, the enhanced solubility and increased efficacy of MPX-004 and MPX-007 suggest that these NAMs could be useful tool compounds with which to study the contributions of GluN2A-containing NMDA receptors to normal brain function and disease (Volkmann et al., 2016). In the past decades, NMDA receptors have been widely considered as important targets for pharmacological intervention in a number of neurological and psychiatric diseases, yet drug discovery efforts have provided relatively few NMDA receptor ligands approved as therapeutic agents. The crystal structures of the binding site for GluN2A-selective NAMs provided in this study provide exciting opportunities for the development of novel classes of allosteric modulators and can reinvigorate efforts to develop new NMDA receptor ligands as treatments in CNS disorders.

Experimental Procedures

DNA constructs and ligands

See Supplemental Experimental Procedures for full details regarding DNA constructs and expression of triheteromeric GluN1/2A$_{C1}$/2B$_{AC2}$ receptors. Glutamate (L-glutamic acid), glycine, and DTT were purchased from Sigma-Aldrich. TCN-201, 7CKA, and DCKA were

purchased from Hello Bio, and MPX-004 and MPX-007 were synthesized as previously described by Volkmann et al. (2016) and provided by Luc Therapeutics, Cambridge, MA.

Two-electrode voltage-clamp recordings

For expression in *Xenopus* oocytes, DNA constructs were linearized by restriction enzymes and used as templates for *in vitro* cRNA transcription. Oocytes were purchased from Xenopus 1 or Ecocyte Bioscience, injected with cRNA, and recordings were performed 2-4 days following cRNA injection at room temperature and at a holding potential of −40 mV as previously described (Hansen et al., 2013). The extracellular recording solution contained (in mM) 90 NaCl, 1 KCl, 10 HEPES, 0.5 $BaCl_2$, 0.01 EDTA (pH 7.4 with NaOH). Oocytes expressing GluN1/2A, GluN1/2B, or triheteromeric GluN1/$2A_{C1}$/$2B_{AC2}$ receptors were injected with 20 nl of 50 mM BAPTA approximately 10-30 min before recordings to prevent activity-dependent increases in response amplitude (Williams, 1993). NAMs were dissolved in DMSO to make 100 mM stock solutions, and the concentration of DMSO was kept constant (< 0.3%) in all recording solutions. NAM concentration ranges were limited by compound solubility and TCN-201, MPX-004, and MPX-007 were used at maximal concentrations of 5, 10, and 30 μM, respectively.

Crystallography of GluN1 and GluN2A LBDs

Constructs for the GluN1 LBD and the fusion protein of the small ubiquitin-like modifier (SUMO) and the GluN2A LBD (SUMO-GluN2A LBD) were expressed in *E. coli* OrigamiB (DE3) cells essentially as previously described (Furukawa et al., 2005; Jespersen et al., 2014). See Supplemental Experimental Procedures for full details.

The isolated GluN1 and GluN2A LBD proteins were mixed at a 1:1 molar ratio and dialyzed against a buffer of (in mM) 10 HEPES (pH 7.0), 100 NaCl, 0.01 glycine, and 1 L-glutamate for 14-18 hours. The dialyzed GluN1 and GluN2A LBD protein mixture were concentrated to 4-7 mg/ml for crystallization. The initial crystallization condition was obtained in commercial screening trials and further optimized with grid screening by expanding the precipitant concentrations in 24-well hanging drop or sitting drop plates. After 2-4 days of equilibration at 20 °C, large rod-shaped crystals were obtained by mixing equal volume of protein complex with 0.2 M ammonium acetate and 16-22% PEG 4000 reservoir solution (final pH 6.2). NAM-bound crystals were obtained by soaking glycine/glutamate-bound crystals against the reservoir solution plus 10 μM L-glutamate and 0.1-1.0 mM of the different NAMs for at least 24 hours. DCKA/NAM-bound crystals were obtained by soaking glycine/glutamate-bound crystals against the reservoir solution plus 10 μM L-glutamate, 1 mM DCKA, and 1mM MPX-007 for at least 48 hours. Crystals were cryoprotected in reservoir solution containing 20% (v/v) glycerol and flash-frozen in a 100K nitrogen gas stream.

Diffraction data were collected at the Advanced Photon System SBC-CAT 19-ID and IMCA-CAT 17-ID beamlines, as well as at the Stanford Synchrotron Radiation Lightsource SSRL-SMB 7-1 and 9-2 beamlines. Images were processed using HKL2000 (Otwinowski and Minor, 1997). The initial phasing map were determined by molecular replacement in PHASER (McCoy et al., 2007) using a published glycine/glutamate-bound GluN1/2A LBD

structure (PDB ID 4NF8; Jespersen et al., 2014) as search model. The initial models of NAM-bound structures were fit into a $2mF_o$-DF_c map with COOT (Emsley et al., 2010) and subjected to one cycle of rigid-body refinement using PHENIX (Adams et al., 2010). Subsequently, the models were further refined by iterative model rebuilding in COOT and refinement with PHENIX. NAM ligands in each structure were located in a mF_o-DF_c map (Read, 1986). Data collection and refinement statistics are shown in Table S2.

Supplementary Material

Refer to Web version on PubMed Central for supplementary material.

Acknowledgements

We thank the staff at the Advanced Photon System (APS), Argonne National Laboratory and the Stanford Synchrotron Radiation Lightsource (SSRL), SLAC National Accelerator Laboratory for their excellent beamline support. The use of SSRL and APS are supported by the U.S. Department of Energy, Office of Science, Office of Basic Energy Sciences under Contract No. DE-AC02-76SF00515 and DE-AC02-06-CH11357. The SSRL Structural Molecular Biology Program is supported by the DOE Office of Biological and Environmental Research, and by the National Institutes of Health (P41GM103393).We thank Hiro Furukawa for providing DNA constructs for expression and purification of GluN1 and GluN2A LBDs, Gabriella K. Popescu for providing the DNA construct for GluN1-CC, and Gina C. Bullard, Marlene E. Woldstad, and Cindee K. Yates-Hansen for excellent technical assistance. We thank Christopher M. Fanger, David R. Anderson, and Ethan Magno for discussion and critical comments. This work was supported by the National Institutes of Health (P20GM103546 and R01NS097536) and a small research grant from Mnemosyne Pharmaceuticals, Inc., which is now Luc Therapeutics, Inc. and holds the patent on MPX-004 and MPX-007. K.B.H. was a paid consultant for Luc Therapeutics and R.A.V. and F.S.M. are shareholders in Luc Therapeutics.

References

Adams PD, Afonine PV, Bunkoczi G, Chen VB, Davis IW, Echols N, Headd JJ, Hung LW, Kapral GJ, Grosse-Kunstleve RW, et al. PHENIX: a comprehensive Python-based system for macromolecular structure solution. Acta Crystallogr. D Biol. Crystallogr. 2010; 66:213–221. [PubMed: 20124702]

Akazawa C, Shigemoto R, Bessho Y, Nakanishi S, Mizuno N. Differential expression of five N-methyl-D-aspartate receptor subunit mRNAs in the cerebellum of developing and adult rats. J. Comp. Neurol. 1994; 347:150–160. [PubMed: 7798379]

Benveniste M, Mayer ML. Kinetic analysis of antagonist action at N-methyl-D-aspartic acid receptors. Two binding sites each for glutamate and glycine. Biophys. J. 1991; 59:560–573. [PubMed: 1710938]

Bettini E, Sava A, Griffante C, Carignani C, Buson A, Capelli AM, Negri M, Andreetta F, Senar-Sancho SA, Guiral L, et al. Identification and characterization of novel NMDA receptor antagonists selective for NR2A-over NR2B-containing receptors. J. Pharmacol. Exp. Ther. 2010; 335:636–644. [PubMed: 20810618]

Bissantz C, Kuhn B, Stahl M. A medicinal chemist's guide to molecular interactions. J. Med. Chem. 2010; 53:5061–5084. [PubMed: 20345171]

Borschel WF, Cummings KA, Tindell LK, Popescu GK. Kinetic contributions to gating by interactions unique to N-methyl-D-aspartate (NMDA) receptors. J. Biol. Chem. 2015; 290:26846–26855. [PubMed: 26370091]

Cheriyan J, Balsara RD, Hansen KB, Castellino FJ. Pharmacology of triheteromeric N-Methyl-D-Aspartate Receptors. Neurosci. Lett. 2016; 617:240–246. [PubMed: 26917100]

Edman S, McKay S, Macdonald LJ, Samadi M, Livesey MR, Hardingham GE, Wyllie DJ. TCN 201 selectively blocks GluN2A-containing NMDARs in a GluN1 co agonist dependent but non-competitive manner. Neuropharmacology. 2012; 63:441–449. [PubMed: 22579927]

Emsley P, Lohkamp B, Scott WG, Cowtan K. Features and development of Coot. Acta Crystallogr. D Biol. Crystallogr. 2010; 66:486–501. [PubMed: 20383002]

Furukawa H, Gouaux E. Mechanisms of activation, inhibition and specificity: crystal structures of the NMDA receptor NR1 ligand-binding core. EMBO J. 2003; 22:2873–2885. [PubMed: 12805203]

Furukawa H, Singh SK, Mancusso R, Gouaux E. Subunit arrangement and function in NMDA receptors. Nature. 2005; 438:185–192. [PubMed: 16281028]

Gielen M, Siegler Retchless B, Mony L, Johnson JW, Paoletti P. Mechanism of differential control of NMDA receptor activity by NR2 subunits. Nature. 2009; 459:703–707. [PubMed: 19404260]

Hackos DH, Lupardus PJ, Grand T, Chen Y, Wang TM, Reynen P, Gustafson A, Wallweber HJ, Volgraf M, Sellers BD, et al. Positive Allosteric Modulators of GluN2A-Containing NMDARs with Distinct Modes of Action and Impacts on Circuit Function. Neuron. 2016; 89:983–999. [PubMed: 26875626]

Hansen KB, Ogden KK, Traynelis SF. Subunit-selective allosteric inhibition of glycine binding to NMDA receptors. J. Neurosci. 2012; 32:6197–6208. [PubMed: 22553026]

Hansen KB, Ogden KK, Yuan H, Traynelis SF. Distinct functional and pharmacological properties of Triheteromeric GluN1/GluN2A/GluN2B NMDA receptors. Neuron. 2014; 81:1084–1096. [PubMed: 24607230]

Hansen KB, Tajima N, Risgaard R, Perszyk RE, Jorgensen L, Vance KM, Ogden KK, Clausen RP, Furukawa H, Traynelis SF. Structural determinants of agonist efficacy at the glutamate binding site of N-methyl-D-aspartate receptors. Mol. Pharmacol. 2013; 84:114–127. [PubMed: 23625947]

Hatton CJ, Paoletti P. Modulation of triheteromeric NMDA receptors by N-terminal domain ligands. Neuron. 2005; 46:261–274. [PubMed: 15848804]

Ishii T, Moriyoshi K, Sugihara H, Sakurada K, Kadotani H, Yokoi M, Akazawa C, Shigemoto R, Mizuno N, Masu M, et al. Molecular characterization of the family of the N-methyl-D-aspartate receptor subunits. J. Biol. Chem. 1993; 268:2836–2843. [PubMed: 8428958]

Jespersen A, Tajima N, Fernandez-Cuervo G, Garnier-Amblard EC, Furukawa H. Structural insights into competitive antagonism in NMDA receptors. Neuron. 2014; 81:366–378. [PubMed: 24462099]

Karakas E, Furukawa H. Crystal structure of a heterotetrameric NMDA receptor ion channel. Science. 2014; 344:992–997. [PubMed: 24876489]

Karakas E, Simorowski N, Furukawa H. Subunit arrangement and phenylethanolamine binding in GluN1/GluN2B NMDA receptors. Nature. 2011; 475:249–253. [PubMed: 21677647]

Kazi R, Dai J, Sweeney C, Zhou HX, Wollmuth LP. Mechanical coupling maintains the fidelity of NMDA receptor-mediated currents. Nat. Neurosci. 2014; 17:914–922. [PubMed: 24859202]

Kussius CL, Popescu GK. NMDA receptors with locked glutamate-binding clefts open with high efficacy. J. Neurosci. 2010; 30:12474–12479. [PubMed: 20844142]

Lee CH, Lu W, Michel JC, Goehring A, Du J, Song X, Gouaux E. NMDA receptor structures reveal subunit arrangement and pore architecture. Nature. 2014; 511:191–197. [PubMed: 25008524]

McCoy AJ, Grosse-Kunstleve RW, Adams PD, Winn MD, Storoni LC, Read RJ. Phaser crystallographic software. J Appl Crystallogr. 2007; 40:658–674. [PubMed: 19461840]

Monyer H, Burnashev N, Laurie DJ, Sakmann B, Seeburg PH. Developmental and regional expression in the rat brain and functional properties of four NMDA receptors. Neuron. 1994; 12:529–540. [PubMed: 7512349]

Otwinowski Z, Minor W. Processing of X-ray diffraction data collected in oscillation mode. Method Enzymol. 1997; 276:307–326.

Paoletti P, Bellone C, Zhou Q. NMDA receptor subunit diversity: impact on receptor properties, synaptic plasticity and disease. Nat. Rev. Neurosci. 2013; 14:383–400. [PubMed: 23686171]

Pierson TM, Yuan H, Marsh ED, Fuentes-Fajardo K, Adams DR, Markello T, Golas G, Simeonov DR, Holloman C, Tankovic A, et al. GRIN2A mutation and early-onset epileptic encephalopathy: personalized therapy with memantine. Annals of clinical and translational neurology. 2014; 1:190–198. [PubMed: 24839611]

Rauner C, Kohr G. Triheteromeric NR1/NR2A/NR2B receptors constitute the major N-methyl-D-aspartate receptor population in adult hippocampal synapses. J. Biol. Chem. 2011; 286:7558–7566. [PubMed: 21190942]

Read RJ. Improved Fourier Coefficients for Maps Using Phases from Partial Structures with Errors. Acta Crystallographica Section A. 1986; 42:140–149.

Sheng M, Cummings J, Roldan LA, Jan YN, Jan LY. Changing subunit composition of heteromeric NMDA receptors during development of rat cortex. Nature. 1994; 368:144–147. [PubMed: 8139656]

Stroebel D, Carvalho S, Grand T, Zhu S, Paoletti P. Controlling NMDA receptor subunit composition using ectopic retention signals. J. Neurosci. 2014; 34:16630–16636. [PubMed: 25505316]

Tovar KR, McGinley MJ, Westbrook GL. Triheteromeric NMDA receptors at hippocampal synapses. J. Neurosci. 2013; 33:9150–9160. [PubMed: 23699525]

Traynelis SF, Wollmuth LP, McBain CJ, Menniti FS, Vance KM, Ogden KK, Hansen KB, Yuan H, Myers SJ, Dingledine R. Glutamate receptor ion channels: structure, regulation, and function. Pharmacol. Rev. 2010; 62:405–496. [PubMed: 20716669]

Vicini S, Wang JF, Li JH, Zhu WJ, Wang YH, Luo JAH, Wolfe BB, Grayson DR. Functional and pharmacological differences between recombinant N-methyl-D-aspartate receptors. J. Neurophysiol. 1998; 79:555–566. [PubMed: 9463421]

Volgraf M, Sellers BD, Jiang Y, Wu G, Ly CQ, Villemure E, Pastor RM, Yuen PW, Lu A, Luo X, et al. Discovery of GluN2A-Selective NMDA Receptor Positive Allosteric Modulators (PAMs): Tuning Deactivation Kinetics via Structure-Based Design. J. Med. Chem. 2016; 59:2760–2779. [PubMed: 26919761]

Volkmann RA, Fanger CM, Anderson DR, Sirivolu VR, Paschetto K, Gordon E, Virginio C, Gleyzes M, Buisson B, Steidl E, et al. MPX-004 and MPX-007: New Pharmacological Tools to Study the Physiology of NMDA Receptors Containing the GluN2A Subunit. PLoS ONE. 2016; 11:e0148129. [PubMed: 26829109]

Williams K. Ifenprodil Discriminates Subtypes of the N-Methyl-D-Aspartate Receptor - Selectivity and Mechanisms at Recombinant Heteromeric Receptors. Mol. Pharmacol. 1993; 44:851–859. [PubMed: 7901753]

Yao Y, Belcher J, Berger AJ, Mayer ML, Lau AY. Conformational analysis of NMDA receptor GluN1, GluN2, and GluN3 ligand-binding domains reveals subtype-specific characteristics. Structure. 2013; 21:1788–1799. [PubMed: 23972471]

Yuan H, Hansen KB, Vance KM, Ogden KK, Traynelis SF. Control of NMDA receptor function by the NR2 subunit amino-terminal domain. J. Neurosci. 2009; 29:12045–12058. [PubMed: 19793963]

Yuan H, Hansen KB, Zhang J, Pierson TM, Markello TC, Fajardo KV, Holloman CM, Golas G, Adams DR, Boerkoel CF, et al. Functional analysis of a de novo GRIN2A missense mutation associated with early-onset epileptic encephalopathy. Nat. Commun. 2014; 5:3251. [PubMed: 24504326]

Yuan H, Low CM, Moody OA, Jenkins A, Traynelis SF. Ionotropic GABA and Glutamate Receptor Mutations and Human Neurologic Diseases. Mol. Pharmacol. 2015; 88:203–217. [PubMed: 25904555]

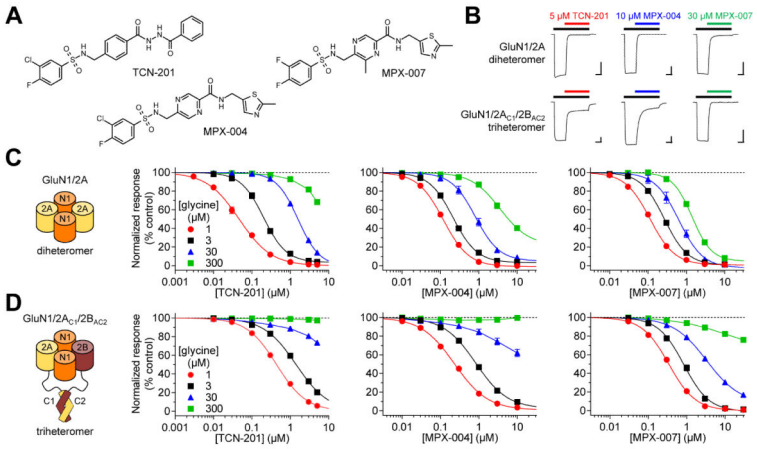

Figure 1. Glycine-sensitivity of inhibition by GluN2A-selective NAMs

A) Chemical structures of GluN2A-selective negative allosteric modulators (NAMs).

B) Representative recordings showing inhibition of diheteromeric GluN1/2A and triheteromeric GluN1/2A/2B receptors by NAMs. Responses are activated by 100 μM glutamate in the continuous presence of 3 μM glycine and recorded using two-electrode voltage-clamp electrophysiology. Triheteromeric GluN1/2A$_{C1}$/2B$_{AC2}$ receptors are expressed without diheteromeric GluN1/2A and GluN1/2B receptors using engineered C1 and C2 tags (Hansen et al., 2014). Horizontal and vertical scale bars represent 1 min and 100 nA, respectively.

C-D) NAM concentration-inhibition data at GluN1/2A receptors comprised of two GluN1 and two GluN2A subunits and GluN1/2A/2B receptors comprised of two GluN1 and two different GluN2 subunits (GluN2A and GluN2B). Inhibition is measured for responses activated by 100 μM glutamate in the continuous presence of 1, 3, 30, or 300 μM glycine. Data are mean ± SEM from 5-14 oocytes.

See also Figures S1 and S2; Table S1.

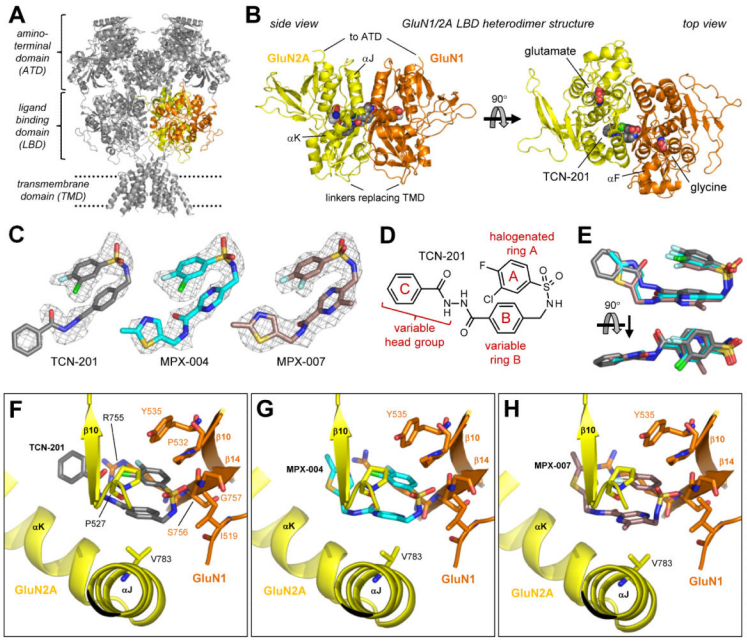

Figure 2. Structures of NAM-bound GluN1/2A LBD heterodimers

A) Structure of the NMDA receptor composed of two GluN1 and two GluN2 subunits (PDB ID 4PE5; (Karakas and Furukawa, 2014). One GluN1/GluN2 LBD heterodimer is highlighted in orange and yellow.

B) Crystal structure of the soluble glycine/glutamate-bound GluN1/2A LBD heterodimer in complex with TCN-201. Expression and purification of soluble NMDA receptor LBDs is made possible by deleting the amino-terminal domain (ATD) and replacing the transmembrane domain (TMD) with a Gly-Thr dipeptide linker.

C) NAM ligands from crystal structures of glycine/glutamate-bound GluN1/2A LBD heterodimers in complex with TCN-201 (2.28 Å), MPX-004 (2.52 Å), and MPX-007 (2.11 Å). The NAM ligands could be unambiguously fitted to their electron densities shown as grey mesh (mF_o-DF_c omit map contoured at 2.5σ).

D) Chemical structures of the NAMs, here exemplified by TCN-201, contain a halogenated ring A, a variable ring B, which is phenyl in TCN-201 and pyrazine in MPX-004/MPX-007, and a variable head group with a ring C that is phenyl in TCN-201 and thiazole in MPX-004/MPX-007.

E) Overlay of TCN-201 (grey), MPX-004 (cyan), and MPX-007 (salmon) from their respective GluN1/GluN2A LBD structures.

F-H) Views of the NAM binding site in structures of the glycine/glutamate-bound GluN1/2A LBD heterodimer in complex with TCN-201 (grey; F), MPX-004 (cyan, G), and MPX-007 (salmon; H). The NAM binding site is formed by residues from β-sheet 10 and α-helices J and K in GluN2A (yellow) and β-sheets 10 and 14 in GluN1 (orange).

See also Figure S4 and Table S2.

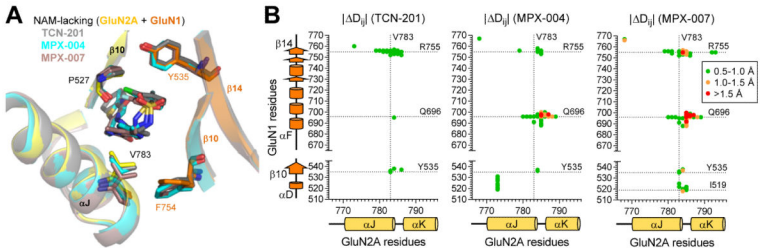

Figure 3. Analysis of NAM-mediated structural changes in GluN1/2A LBD structures

A) Structural alignment of the NAM binding site in the GluN1/2A LBD heterodimer without bound NAM (yellow and orange) and in complex with TCN-201 (grey), MPX-004 (cyan), and MPX-007 (salmon).

B) Difference distance maps showing pairs of Cα atoms that are less than 15 Å apart in the NAM-lacking structure and change by more than 0.5 Å in NAM-bound structures. The difference distance $|\Delta D_{ij}|$ is the absolute value of the distance measured in the NAM-lacking structure minus the distance measured in the NAM-bound structure.

See also Figure S5.

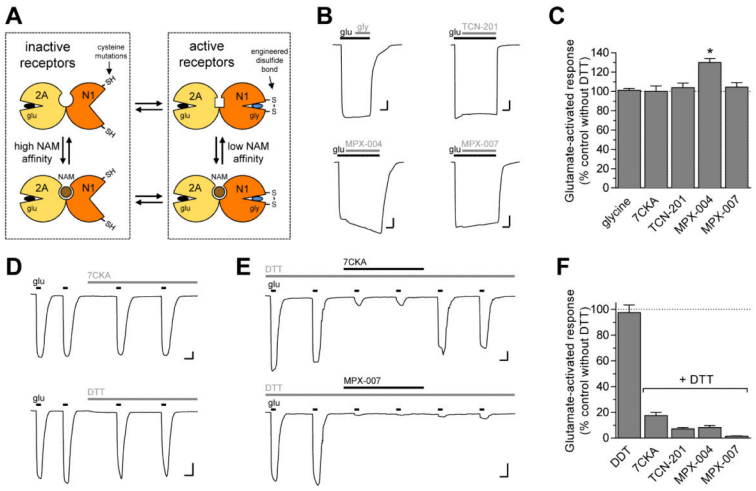

Figure 4. Relationship between NAM inhibition and the GluN1 LBD conformation

A) Cartoon illustrating conformations of the GluN1/2A LBD heterodimer with the NAM binding site in the subunit interface. In this cartoon, glutamate is continuously bound to the GluN2A LBD and glycine must induce a closed GluN1 LBD conformation for NMDA receptor activation. The cartoon also depicts the engineered disulfide bond introduced by N499C + Q686C mutations in GluN1 (GluN1-CC).

B) Representative two-electrode voltage-clamp recordings of responses from GluN1-CC/2A receptors with the GluN1 LBD locked in the closed, active conformation. Reponses are activated by 100 μM glutamate alone, followed by co-application of glycine (300 μM), TCN-201 (5 μM), MPX-004 (10 μM), or MPX-007 (30 μM). Horizontal and vertical scale bars represent 30 sec and 50 nA, respectively.

C) Summary of the effects of glycine (300 μM), the competitive glycine-site antagonist 7CKA (10 μM), TCN-201 (5 μM), MPX-004 (10 μM), and MPX-007 (30 μM) on glutamate-activated responses from GluN1-CC/2A receptors. Data are mean ± SEM from 5-6 oocytes. * indicates significantly different from all other groups ($P < 0.05$; one-way ANOVA with Tukey-Kramer posttest).

D-E) Representative recordings of responses from GluN1-CC/2A receptors activated by 100 μM glutamate alone. Co-application of DTT (4 mM) plus the competitive antagonist 7CKA (10 μM) or MPX-007 (30 μM) diminished glutamate-activated responses. Horizontal and vertical scale bars represent 1 min and 100 nA, respectively.

F) Summary of the effects of DTT alone (4 mM) and co-application of DTT plus 7CKA (10 μM), TCN-201 (5 μM), MPX-004 (10 μM), or MPX-007 (30 μM) on glutamate-activated responses from GluN1-CC/2A receptors. Data are mean ± SEM from 5-24 oocytes

See also Figure S6.

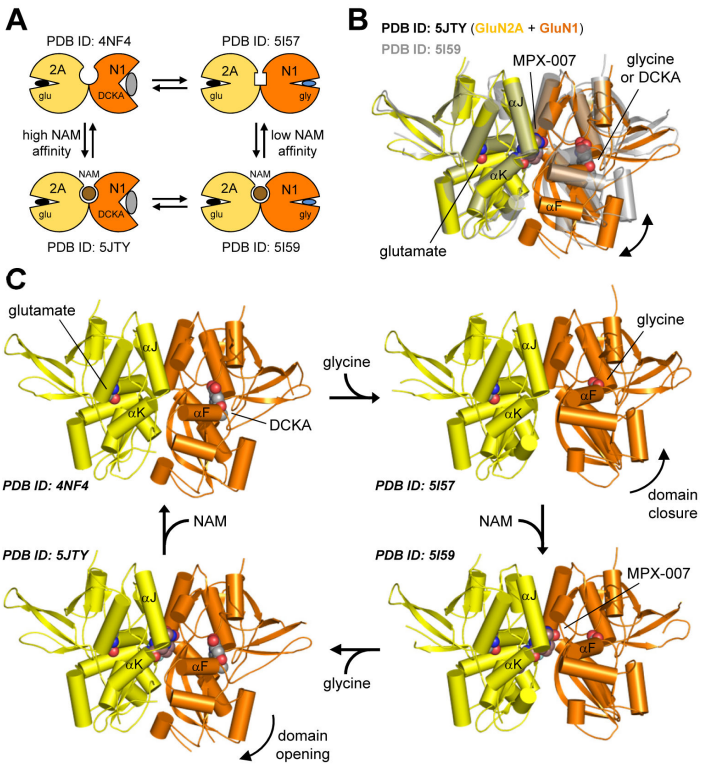

Figure 5. Crystal structures of conformational states in the NAM inhibition cycle

A) Cartoon illustrating conformations of the GluN1/2A LBD heterodimer in the NAM inhibition cycle. In this cartoon, glutamate is continuously bound to the GluN2A LBD and the competitive glycine-site antagonist DCKA stabilizes the open (i.e. glycine-lacking) state of the GluN1 LBD. PDB IDs of structures corresponding to the four conformations are listed.

B) Overlay of DCKA/glutamate-bound (PDB ID 5JTY; yellow and orange) and glycine/glutamate-bound (PDB ID 5I59; grey) structures in complex with MPX-007, illustrating the difference in GluN1 LBD domain closure (indicated by the arrow).

C) Crystal structures of the GluN1/2A LBD heterodimer corresponding to conformational states in the NAM inhibition cycle. Arrows indicate transitions between states and structural changes.

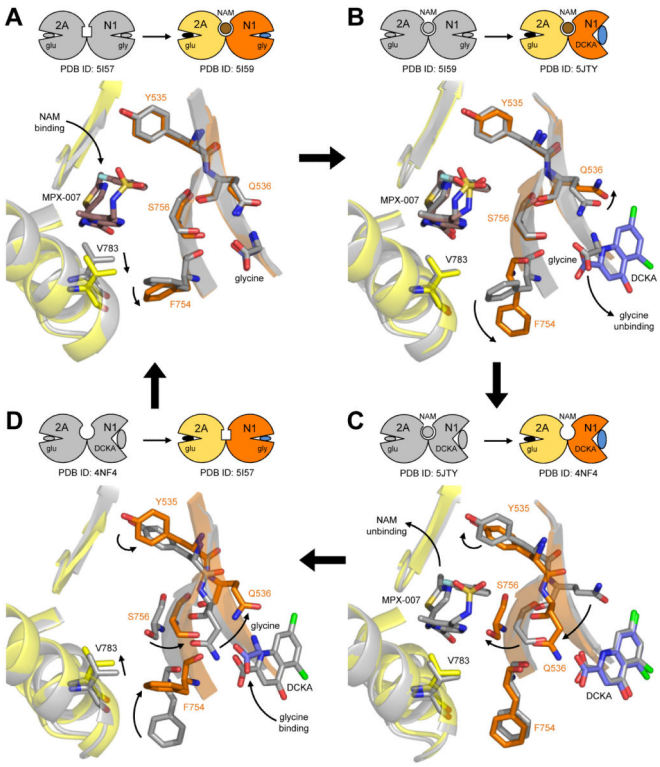

Figure 6. Structural changes in the NAM binding site during allosteric inhibition

A) Structural changes in modulatory binding site upon NAM binding to the glycine/glutamate-bound GluN1/2A LBD heterodimer. Binding of NAM (i.e. MPX-007) displaces GluN2A V783 and this “push” is accompanied by a steric effect on GluN1 F754.

B) Structural changes upon glycine unbinding from the NAM-bound GluN1/2A LBD heterodimer. Glycine unbinding and opening of the GluN1 LBD (here stabilized by DCKA) enable a conformational change of GluN1 F754, removing steric interaction with GluN2A V783.

C) Structural changes upon NAM unbinding from the DCKA/glutamate-bound GluN1/2A LBD heterodimer. NAM unbinding enables a relaxation of residues in the GluN1 hinge region.

D) Structural changes upon glycine binding to the NAM-lacking GluN1/2A LBD heterodimer. Glycine binding and closure of the GluN1 LBD reengages the steric interaction between GluN2A V783 and GluN1 F754, and places residues in the GluN1 hinge region in a conformation permissive for NAM binding.

See also Figure S7.

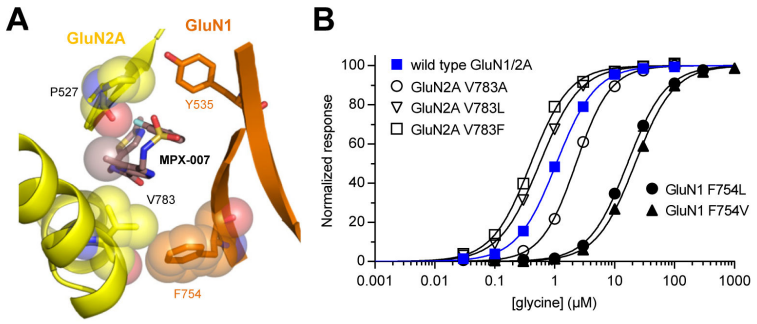

Figure 7. Mutational analyses of the influence of GluN2A V783 and GluN1 F754 on glycine potency

A) View of the NAM binding site in the glycine/glutamate-bound GluN1/2A LBD heterodimer in complex with MPX-007. The van der Waals radius of the methyl group of MPX-007 is shown as transparent sphere. This methyl group contacts the backbone carbonyl of GluN2A P527 and the side chain of GluN2A V783. There is also a nonpolar interaction between side chains of GluN2A V783 and GluN1 F754.

B) Glycine concentration-response data for wild type and mutated GluN1/2A receptors. Responses are recorded in the presence of 100 μM glutamate using two-electrode voltage-clamp electrophysiology. Data are mean ± SEM from 9-16 oocytes.

See also Table S3.

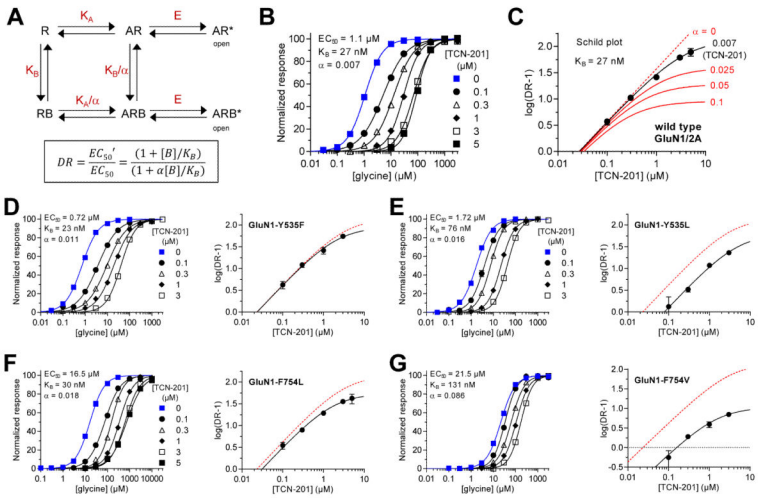

Figure 8. Evaluation of GluN1 Y535 and F754 in allosteric inhibition of glycine binding

A) Operational model for TCN-201 inhibition by allosteric modulation of glycine binding without changing agonist efficacy (E). A is the agonist glycine, B is the NAM, and R is the receptor. Agonist binding affinity (K_A) is changed by an allosteric constant α upon NAM binding, and NAM binding affinity (K_B) is changed by α upon agonist binding. The equation for the dose ratio DR, the ratio of agonist EC_{50} values in presence and absence of modulator, is shown.

B) Glycine concentration-response data for GluN1/2A in the absence or presence of TCN-201 are analyzed by simultaneously fitting all data to both the dose ratio DR equation and the Hill equation using global nonlinear regression, yielding the glycine EC_{50}, TCN-201 binding affinity (K_B), and allosteric constant α that describe all the experimental data.

C) DR values derived from fitting individual concentration-response data shown in B) are plotted as a function of TCN-201 concentration in the Schild plot, which also illustrates the effects of changing the allosteric constant α, but with constant K_B (27 nM). The black line is generated using the K_B and α obtained by fitting all data in B) using global nonlinear regression (i.e. the black line is not obtained by fitting directly to DR values). Competitive antagonists have $\alpha = 0$ (dashed line).

D-G) Schild analysis of TCN-201 inhibition for mutated GluN1/2A receptors. Glycine concentration-response data are analyzed using global nonlinear regression (left side) and the resulting binding affinity (K_B) and allosteric constant (α) are used to generate the black line in the Schild plot (right side) with the corresponding DR values. Dashed red line indicates the Schild plot for wild type GluN1/2A receptors.

See also Figures S1 and S8; Table S3.